Oriented covalent organic framework film on graphene for robust ambipolar vertical organic field-effect transistor

Bing Sun[1,2], Chen-Hui Zhu,[3] Yi Liu,[3-4] Cheng Wang,[4] Li-Jun Wan[1], Dong Wang[1]

1 Key Laboratory of Molecular Nanostructure and Nanotechnology, Institute of Chemistry, Chinese Academy of Sciences (CAS), Beijing 100190, P. R. China

2 University of CAS, Beijing 100049, P. R. China

3 Advanced Light Source, Lawrence Berkeley National Laboratory, Berkeley, CA 94720, USA

4 The Molecular Foundry, Lawrence Berkeley National Laboratory, Berkeley, CA 94720, USA

4 Key Laboratory of Biomedical Polymers (Ministry of Education), College of Chemistry and Molecular Sciences, Wuhan University, Wuhan 430072, China.

Correspondence and requests for materials should be addressed to D.W. (email: wangd@iccas.ac.cn).

Abstract

Periodically eclipsed π-stacking columns in two-dimensional covalent organic frameworks (2D COFs) could function as direct channel paths for charge carrier transport. Incorporating a well-defined 2D COF into organic electronic devices, however, is still a challenge. Herein, we reported the solvothermal synthesis of a $COF_{TFPy\text{-}PPDA}$ film on single layer graphene (SLG), which was constructed via covalent imine-type linkage by employing 1,3,6,8-tetrakis(*p*-formylphenyl)pyrene (TFPy) and *p*-phenylenediamine (PPDA) as building blocks. A vertical field-effect transistor (VFET) based on the heterostructure of $COF_{TFPy\text{-}PPDA}$ film and SLG shows ambipolar charge carrier behavior under lower modulating voltages. Work-function-tunable contact between SLG and $COF_{TFPy\text{-}PPDA}$ film and suitable injection barriers of charge carriers lead to the ambipolar transport with high current density on/off ratio ($>10^5$) and high on-current density (>4.1 Acm^{-2}). Interfacing 2D COF with graphene for VFET could shed the promising application prospect of 2D COFs in organic electronics and optoelectronics.

Semiconducting π-conjugated systems incorporated with versatile functionalities by molecular design have attracted much attention as intriguing and advanced materials in organic electronics and optoelectronics[1-3]. The charge transport efficiency is considered the utmost essential factor for high performance electronic devices. It in turn largely depends on the molecular packing mode and intermolecular interaction between neighboring molecules as well as the chemical structure of π-conjugated organic semiconductors[4]. In general, the maximum π-overlap in an orderly packed molecular system are regarded as the most efficient mode for charge transport[5]. Two-dimensional covalent organic frameworks (2D COFs), which are covalently constructed from planar aromatic building blocks based on the principles of reticular chemistry, are a class of porous crystalline material with the highly ordered porous architectures and predesignable π-electronic skeletons. 2D COFs feature the extended conjugation within a 2D layer and periodical columnar π-arrays aligned with an atomic precision in vertical direction, which is hardly achievable in other molecular architectures[6-9]. In this context, high crystallinity and closely eclipsed stacking alignment of aromatic moieties render 2D COFs as an ideal platform for charge carrier transport[10]. By carefully choosing suitable π-functional monomers, semiconducting 2D COFs have been developed with tunable charge-transfer performance[11-13]. For example, p-type 2D COFs for hole transport were reported based on the monomers containing electron-rich units such as pyrene, porphyrin, phthalocyanine and tetrathiafulvalene[14-17]. Electron-transporting 2D COFs with n-channels were also constructed by co-condensation of nickel-phthalocyanine with an electron-deficient benzothiadiazole block[11]. Ambipolar semiconducting 2D COFs were fabricated from various electron donor and electron acceptor components[10,12,18]. Some of these 2D COFs were revealed to have high spectroscopic carrier mobility by using a flash photolysis time-resolved microwave

conductivity method[11,12,15,19]. However, the lack of solution processability due to the inherent insolubility of COF powders impedes their integration into devices. Furthermore, the application of 2D COF powders in the organic solar cells has been also explored[20,21].

Growing crystalline 2D COF thin film on an appropriate substrate is considered as one of the efficient ways to fabricate COF-based devices[22-25]. With the assistance of substrates, on-surface grown COF films have been demonstrated to form preferentially oriented 2D layers parallel to substrate surface and vertically aligned π-columns[22,26]. This film geometry provides unidirectional channels for improved charge migration along π-columns. For instance, oriented crystalline DAAQ-TFP COF film showed the drastically improved charge storage capabilities compared with randomly oriented DAAQ-TFP COF powders[27]. Another example is that 2D BDT-COF film with highly ordered π-arrays and porous structures could serve as hosts for forming periodically interpenetrated electron-donor/acceptor system to effectively separate and transport charge carriers[23]. With the improved crystallinity and orientation control, substrate supported 2D COF film would enable fabrication of advanced architectures for electronic devices, which however remains unexplored so far.

Vertical field-effect transistor (VFET) is a rapidly developed electronic device which is fabricated by vertically stacking source electrode, channel layer and drain electrode on gate insulator[28,29]. The short channel length in nano-scale or micro-scale can be tuned by simply controlling the thickness of deposited semiconducting layer. This device structure intrinsically allows the possibility for low-power and low-voltage manipulation, high current outputs and is compatible with exquisite lithography processes. Recently, single-layered graphene (SLG) is extensively utilized as a superior source electrode in VFETs[30-32]. High device performances of this

kind VFET architecture are obtained due to the intrinsic advantages of graphene, including i) improved sheet resistance, ii) monoatomic layered thickness allowing the gate field accessible to the graphene-semiconductor interface for charge accumulation, iii) low density of state and dramatically tunable work function for carrier injection and current modulation, iv) gate-tunable interfacial resistance between graphene and a semiconductor achieving a high on/off ratio[33-35]. The graphene-based VFET provides a new way to investigate the electrical properties of semiconductors and promise the rational design and realization of flexible and large-area electronics in active matrix displays or low-power logic applications[36]. Inspired by the oriented growth of 2D COF film on SLG surface and the inherent periodic π-arrays of 2D COFs, it is intriguing to incorporate 2D COF film/SLG into VFETs for exploring its intrinsic electronic performances and potential applications.

Herein, we constructed an imine-based $COF_{TFPy\text{-}PPDA}$ thin film from 1,3,6,8-tetrakis(*p*-formylphenyl)pyrene (TFPy) and *p*-phenylenediamine (PPDA) on SLG surface and fabricated a VFET device based on the SLG/COF film heterostructure (**Fig. 1**). A 1,3,6,8-tetrasubstituted pyrene molecule, TFPy, was chosen as a building block due to its high carrier mobility in organic electronics and optoelectronics[37]. The imine-based $COF_{TFPy\text{-}PPDA}$ thin film was revealed to have the well-defined structure and good crystallinity. In the VFET architecture, SLG served as the source electrode and the deposited Au electrode as the drain electrode (**Fig. 1c**). By employing $COF_{TFPy\text{-}PPDA}$ film as the semiconducting layer, the VFET device displayed ambipolar charge carrier transport behavior modulated effectively by monitoring gate voltages. A high $J_{on\text{-}off}$ ratio greater than 10^5 was achieved at a lower manipulating voltage. The maximum on-current density can be reached to 6.8 A cm^{-2} for hole delivering and 4.1 A cm^{-2} for electron transporting. This COF-based VFET provides a universal method to investigate the electronic properties of highly ordered 2D COF films. The

excellent semiconducting performance of COF-based VFETs promises new possibility for their applications of COF in organic electronics.

Results

Synthesis and spectroscopic characterization of $COF_{TFPy\text{-}PPDA}$ film on SLG. The $COF_{TFPy\text{-}PPDA}$ film on SLG was constructed through a typical solvothermal procedure using a mixed solvent of dioxane/methanol (3:1, v/v). The chemical structure of $COF_{TFPy\text{-}PPDA}$ film was confirmed by using Fourier transform infrared spectroscopy (FTIR) and confocal Raman spectra. FTIR spectra of $COF_{TFPy\text{-}PPDA}$ film and powders indicate the complete consumption of monomers (**Fig. 2a**), as the characteristic stretching band (1700 cm^{-1}) of aldehyde groups in TFPy remarkably decreases and the stretching band (3200 – 3400 cm^{-1}) of amino groups in PPDA is absent. The emerging characteristic peak at 1622 cm^{-1} is ascribed to the stretching mode of the formed imine bond (C=N) in $COF_{TFPy\text{-}PPDA}$ film as well as that in COF powders.

Further structural information is confirmed by Raman spectra as shown in **Fig. 2b**. By comparing the Raman spectrum of bulk $COF_{TFPy\text{-}PPDA}$ with that of monomers, the broad band at 1696 cm^{-1} corresponding to aldehyde C=O stretching vibration and the band at 1276 cm^{-1} indexed as the stretching and wagging vibration of NH_2 in PPDA are absent in the case of $COF_{TFPy\text{-}PPDA}$[38]. The emerging bands at 1573 and 1651 cm^{-1} correspond to stretching vibrations of newly formed imine moieties [24] and the band at 1610 cm^{-1} is inherited from the vibration mode of pyrene core. In addition, the SLG transferred onto silicon wafer shows the typical G band at 1576 cm^{-1} and 2D band at 2682 cm^{-1} [39]. The $COF_{TFPy\text{-}PPDA}$ film growing on SLG possesses a similar Raman spectrum comparing with that of bulk powders, also integrating with the broad band at 2680 cm^{-1} deriving

from SLG. The results indicate the covalent formation of imine-connected conjugated structure in both $COF_{TFPy\text{-}PPDA}$ film and powders. Particularly, the Raman spectrum of $COF_{TFPy\text{-}PPDA}$ film demonstrates the increased intensity and slight shifts of some bands (mainly from 1573 to 1581 cm^{-1} and 1610 to 1600 cm^{-1}) comparing to that of $COF_{TFPy\text{-}PPDA}$ powders. It likely arises from the geometrical orientation change of molecules induced by SLG substrate based on surface selection rule[40].

Crystalline structure and orientation characterization. The ordered structure and crystallinity of $COF_{TFPy\text{-}PPDA}$ thin film were investigated by grazing incidence wide angle X-ray scattering (GIWAXS). As shown in **Fig. 3a**, the scattering peaks at q_{xy} = 0.27 $Å^{-1}$, 0.38 $Å^{-1}$, 0.54 $Å^{-1}$, 0.62 $Å^{-1}$, 0.81 $Å^{-1}$ and 1.09 $Å^{-1}$ correspond to (110), (020), (220), (130), (330) and (440) planes, respectively (Supplementary **Fig. S1**). The in-plane plotting spectrum for $COF_{TFPy\text{-}PPDA}$ thin film (**Fig. 3c**) is well consistent with the simulated pattern in eclipsed conformation according to the previous work[41], which reveals the formation of the highly crystalline materials with periodic π-columns[22]. These peaks shown in GIWAXS pattern are almost concentrated near q_Z = 0 which indicates the *c*-axis preferential orientation of polycrystalline $COF_{TFPy\text{-}PPDA}$ film normal to SLG substrate. The significant (001) peak at q_Z = 1.72 $Å^{-1}$ (**Fig. 3b**) is not observed in q_{xy} direction, again indicating the oriented stacking of conjugated layers along *c*-axis due to the π-stacking interaction between SLG and the aromatic pyrene core ~~each other~~. These results reasonably demonstrate the ordered structure of crystalline $COF_{TFPy\text{-}PPDA}$ film formed on SLG surface.

Surface and thickness analysis of $COF_{TFPy\text{-}PPDA}$ thin film. Based on fully conjugated and crystalline $COF_{TFPy\text{-}PPDA}$ film grown on SLG, the SLG/COF-VFET was fabricated and measured at

ambient conditions. SLG transferred onto SiO_2-Si surface cooperating with the remote Au/Cr pads was regarded as bottom source electrode, and top Au pad (100 × 100 μm^2) served as drain electrode. The vertical height of $COF_{TFPy\text{-}PPDA}$ film was regarded as the channel length. The thickness of $COF_{TFPy\text{-}PPDA}$ film is essential to the performance of SLG/COF-VFET devices. **Fig. 4** shows the surface analysis of $COF_{TFPy\text{-}PPDA}$ film on SLG by using atomic force microscopy (AFM). The typical AFM topography image depicts that the flat $COF_{TFPy\text{-}PPDA}$ film can continuously grow on SLG in the solvothermal procedure (**Fig. 4a**). Based on the cross-section analysis as shown in **Fig. 4b**, the average thickness of $COF_{TFPy\text{-}PPDA}$ film is evaluated as 50.5 ± 7.2 nm at monomer concentrations of 5 mM for TFPy and 10 mM for PPDA, respectively. In a lower monomer concentration (1 mM for TFPy and 2 mM for PPDA), thin $COF_{TFPy\text{-}PPDA}$ film with the thickness of only 15.5 ± 1.3 nm is obtained with some breakages (Supplementary **Fig. S2**). When the monomer concentration increased to 2 mM for TFPy, $COF_{TFPy\text{-}PPDA}$ film can cover all the surface of SLG (Supplementary **Fig. S3**). From 2 mM to 5 mM based on TFPy blocks, the thickness of $COF_{TFPy\text{-}PPDA}$ film varies in a narrow range (47 – 55 nm). By virtue of the flatness of SLG, ultrathin channel length (sub-100 nm) could be permitted without electrical shorts to top drain electrode[42]. In our work, full-covering $COF_{TFPy\text{-}PPDA}$ film with the thickness of 50 nm in average was utilized for the characterization of SLG/COF-VFET device.

Electrical transporting performance of the fabricated SLG/COF-VFET. Electrical transport studies of the COF-based VFET were performed and the results are shown in **Fig. 5**. The transistor operation shown in **Fig. 5a** demonstrates the large modulation of drain-source current density (J_{DS})

by the gate voltage (V_G) monitoring in the range of 2 V – -10 V, which mimics p-type transistor behavior with high holes mobility. By virtue of the vertical structure and thin semiconducting layer, the SLG/COF-VFET can be operated under a low drain-source voltage (V_{DS}) of -0.5 V. High on−off current density ($J_{on/off}$) ratio of 10^6 and low threshold voltage (0.1 V) can be obtained. By varying the applied V_{DS} to -1.0 V, a higher on-current density is recorded with the large $J_{on/off}$ ratio maintained. The low off-state current density (below 10^{-5} A cm^{-2}) and low leakage current (confined to the nanoampere range) at on-state also demonstrate the enhanced performance of SLG/COF-VFET devices. Intriguingly, the COF-based VFET also shows the high on-current density when the gate voltage is manipulated in the range of -1 V – 10 V at the V_{DS} of 0.5 V, indicating that $COF_{TFPy\text{-}PPDA}$ film can also acts as n-type channel for electron delivering. The $J_{on/off}$ ratio in the n-type regime can reach to 10^5, while the power consumption is higher than that in the p-type regime, which may be attributed to the intrinsic higher hole mobility than that of electrons. Similar enhanced on-current density is also recorded by altering the applied V_{DS}.

Output characteristics of the COF-based VFET also illustrate the ambipolar behavior of $COF_{TFPy\text{-}PPDA}$ film as shown in **Fig. 5b**. The on-current density can achieve 6.8 A cm^{-2} in p-type regime at the V_{DS} of -10 V with supplied gate voltage of -5 V and 4.1 A cm^{-2} in n-type regime at the V_{DS} of 10 V with supplied gate voltage of 5 V. The discrepant on-current density obtained in two regimes also arises from the different mobility of holes and electrons in the $COF_{TFPy\text{-}PPDA}$ film. Statistical data shown in Supplementary **Table S1** reveal the reproducibility of our SLG/COF-VFET devices. The on-current density for hole and electron transport is among the highest reported values for VFETs (Supplementary **Table S2**), which is ~~beneficial~~beneficial to drive organic light-emitting diode (OLED) devices[30]. The performance of SLG/COF-VFETs can be further improved by

optimizing the structure of COF films, perforating the graphene-based source electrode and altering the drain electrode with different work function.

In order to understand possible mechanism of the ambipolar manipulation for the SLG/COF-VFET, we investigated the ~~electric~~ electronic structure of semiconducting $COF_{TFPy\text{-}PPDA}$ by using cyclic voltammetry (CV) and absorption spectra (Supplementary **Fig. S4 and S5**) to determine the positions of its highest occupied molecular orbitals (HOMO) and lowest unoccupied molecular orbital (LUMO). For $COF_{TFPy\text{-}PPDA}$, HOMO and LUMO levels are evaluated as -5.22 eV and -3.54 eV, respectively, which reveals reduced band-gap compared to TFPy molecule (**Fig. 6a**) due to extended in-plane conjugation. The schemetic bond diagrams shown in **Fig. 6b** demonstrate that the work function positions of SLG (~ -4.7 eV) and Au (~ -5.1 eV) are located between the HOMO and LUMO levels of $COF_{TFPy\text{-}PPDA}$, which can lower the injection barriers for both electrons and holes. The narrow band-gap of $COF_{TFPy\text{-}PPDA}$ (1.61 eV) can also contribute to lower the injection barrier for both charge carriers.

Discussions

In general, the work function or doping level of graphene can be dramatically modulated under appropriate gating voltage[34,36,43]. Furthermore, graphene also ~~processes~~ possesses highly tunable density of state for majority carriers[44]. In the SLG/COF-VFET arrchitecture, gate field as well as the parallel source-drain field can facilitate the accumulation of majority carriers and thus dominate the band diagrams at the interface between SLG and COF film. Under the applied V_G and V_{DS}, the majority carriers tend to selectively inject to the adjacent semiconductor layer[33]. With the gate voltage monitored to negative direction, accumulated holes increase the work function of SLG and

the barrier height between SLG and COF film is reduced, thus resulting in holes injection to the HOMO level of $COF_{TFPy\text{-}PPDA}$ film (**Fig. 6c**). At the negative V_{DS}, the device reveals enhanced current density and is switched ~~into~~ to on-state. The π-columns act as p-type channel for hole~~s~~ transport. The current density under positive V_{DS} is much smaller than that under negative V_{DS} (under negative V_G in **Fig. 5b**), indicating the relatively smaller barrier between SLG and $COF_{TFPy\text{-}PPDA}$ film compared to that between Au and $COF_{TFPy\text{-}PPDA}$ film. Similarly, a positive V_G accumulates electrons in graphene decreasing the work function of SLG to the LUMO level of $COF_{TFPy\text{-}PPDA}$ film, and then the injected electrons into semiconducting COF film deliver to top drain electrode at the positive V_{DS} (n-type current, **Fig. 6d**). Judging from the energy level of $COF_{TFPy\text{-}PPDA}$ (E_{HOMO} < -5 eV and E_{LUMO} < -4 eV), the suitable barriers of both electron and hole from top Au electrode (work function in the range of -4.7 − -5.2 eV) ~~is~~ also allow~~s~~ stable hole~~s~~ and electron~~s~~ transport[45,46], and efficiently facilitate~~s~~ the ambipolar transport. Additionally, the higher power consumption and lower $J_{on/off}$ ratio in n-type regime compared with that in p-type regime may be ascribed to the larger electron injection barrier height than that for holes result~~ed~~ing from the differences of initial graphene Fermi level relative to LUMO and HOMO level, respectively, as well as the intrinsic~~ally~~ electrical properties of $COF_{TFPy\text{-}PPDA}$.

In summary, we constructed the imine-based $COF_{TFPy\text{-}PPDA}$ film with high crystallinity and ordered π-arrays on SLG via a convenient solvothermal method and incorporated them into a VFET by employing $COF_{TFPy\text{-}PPDA}$ film as the transport channel and SLG as the source electrode. Based on the heterostructure of crystalline $COF_{TFPy\text{-}PPDA}$ film and conductive SLG, the SLG/COF-VFET displayed an excellent ambipolar charge transport behavior under the modulation of supplied voltages, which may be ascribed to the tunable work function and density of state of SLG as well as

lower injection barriers for electrons and holes injection. The narrow band-gap of $COF_{TFPy\text{-}PPDA}$ (1.61 eV) can also contribute to lower the injection barrier for both charge carriers. High $J_{on/off}$ ratio of 10^6 in p-type regime and 10^5 in n-type regime were obtained at low manipulating voltages. The highest on-current density could achieve 6.8 A cm^{-2} for holes transporting and 4.1 A cm^{-2} for electrons delivering. The high semiconducting performance and excellent ambipolar behavior of $COF_{TFPy\text{-}PPDA}$ film demonstrate its application prospect in advanced driving cells of OLEDs and flexible organic electronic devices. This unique VFET architecture also provides a universal method to investigate the intrinsic electrical properties of other COF materials and sheds their prospect in electronics and optoelectronics.

Methods

Graphene growth, transfer and source electrode preparation. Single layer graphene (SLG) was first grown on copper foils (25 μm thick, Alfa Aesar, item no. 13382) by chemical vapor deposition (CVD) method and was transferred to silicon wafer with 300 nm fused oxide layer (SiO_2-Si) via the wet transferring method according to our previous work[47]. Remote Au/Cr source electrode (40 nm/6 nm) contacts were evaporated directly onto the edge of transferred SLG electrode on SiO_2/Si substrates.

Growing $COF_{TFPy\text{-}PPDA}$ film on SLG. 1,3,6,8-Tetrakis(*p*-formylphenyl)pyrene (TFPy) was synthesized according to the previous work[48]. ^{1}H NMR (300 MHz, $CDCl_3$, δ): 10.16 (s, 4H, Ar H), 8.17 (s, 4H, Ar H), 8.08 (d, J = 6 Hz, 8H, Ar H), 8.04 (s, 2H, Ar H), 7.86 (d, J = 6 Hz, 8H, Ar H). In a typical procedure, *p*-phenylenediamine (PPDA, Acros Organics), TFPy (with the molar ration of TFPy to PPDA as 2:1) and a mixture of 1,4-dioxane/methanol (v/v 3:1, 1 mL) were charged in a

cylindrical tube (18 cm of length, ϕ_{in} = 8 mm, ϕ_{out} = 10 mm). The mixture was ultrasonic treated to obtain a homogeneous suspension and desaerated with inert argon. After being added 100 μL 3 M acetic acid aqueous solution and SLG/SiO_2-Si slice with Au/Cr (40/6 nm) source electrodes (Supplementary Experimental Details), the tube was sealed and heated in a 120 °C oven for 24 h. After cooled down naturally to room temperature, the substrate slice was picked out and submerged in THF/chloroform (v/v 1:1, 10 mL) overnight and finally rinsed by acetone and dried under vacuum. The precipitates were also collected by centrifugation, rinsed by THF and soaked in THF/chloroform (v/v 1:1, 10 mL) for 12 h, and finally dried under vacuum conditions. Similarly, $COF_{TFPy\text{-}PPDA}$ powders were synthesized in the absence of substrates.

VFET fabrication and measurements. The VFET was fabricated by depositing 60 nm thick Au drain electrode on the surface of $COF_{TFPy\text{-}PPDA}$ film/SLG/SiO_2-Si slice with a shadow mask. *I–V* characteristics of the transistor were recorded on a Keithley 4200 SCS and a Micromanipulator 6150 probe station in a clean and shielded box at ambient atmosphere.

General characterizations. The structures of both $COF_{TFPy\text{-}PPDA}$ films and powders were characterized by X-ray diffraction (XRD), Raman spectra, and Fourier transformation infrared (FTIR) spectra. FTIR spectra were recorded with a Bruker RFS100/S instrument in the range of 600 to 3600 cm^{-1} with an interval of 4 cm^{-1}. FTIR spectrum of $COF_{TFPy\text{-}PPDA}$ films was particularly recorded on a ThermFisher Scientific Nicolet iN10 instrument after cooling the measurement system by using liquid nitrogen for 20 min. Raman spectra were recorded on a Thermo Scientific DXR Raman spectroscopy with 633-nm laser. Grazing incidence wide angle X-ray scattering (GIWAXS) was conducted at Beamline 7.3.3 at the Advanced Light Source (ALS), Lawrence Berkeley National Laboratory, using an approximately 0.5 mm wide 10 keV X-ray beam (λ =

1.2398 Å). The surface characterization of COF films was performed on a Bruker Nanoscope IIIa atomic force microscopy (AFM) in tapping mode at ambient temperature.

References

1. Guo X, Baumgarten M, Müllen K. Designing π-conjugated polymers for organic electronics. *Prog. Polym. Sci.* **38**, 1832-1908 (2013).
2. Ye L, Zhang S, Huo L, Zhang M, Hou J. Molecular design toward highly efficient photovoltaic polymers based on two-dimensional conjugated benzodithiophene. *Acc. Chem. Res.* **47**, 1595-1603 (2014).
3. Cai SL, Zhang WG, Zuckermann RN, Li ZT, Zhao X, Liu Y. The organic flatland-recent advances in synthetic 2D organic layers. *Adv. Mater.* **27**, 5762-5770 (2015).
4. Nan G, Shi Q, Shuai Z, Li Z. Influences of molecular packing on the charge mobility of organic semiconductors: From quantum charge transfer rate theory beyond the first-order perturbation. *Phys. Chem. Chem. Phys.* **13**, 9736-9746 (2011).
5. Wang C, Dong H, Hu W, Liu Y, Zhu D. Semiconducting p-conjugated systems in field-effect transistors: A material odyssey of organic electronics. *Chem. Rev.* **112**, 2208-2267 (2012).
6. Waller PJ, Gandara F, Yaghi OM. Chemistry of covalent organic frameworks. *Acc Chem Res* **48**, 3053-3063 (2015).
7. Lukose B, Kuc A, Frenzel J, Heine T. On the reticular construction concept of covalent organic frameworks. *Beilstein J. Nanotechnol.* **1**, 60-70 (2010).
8. Ding S-Y, Wang W. Covalent organic frameworks (COFs): From design to applications. *Chem. Soc. Rev.* **42**, 548-568 (2013).
9. Dogru M, Bein T. On the road towards electroactive covalent organic frameworks. *Chem. Commun.* **50**, 5531-5546 (2014).
10. Jin S, *et al.* Creation of superheterojunction polymers via direct polycondensation: Segregated and bicontinuous donor-acceptor π-columnar arrays in covalent organic frameworks for long-lived charge separation. *J. Am. Chem. Soc.* **137**, 7817-7827 (2015).
11. Ding X, *et al.* An n-channel two-dimensional covalent organic framework. *J. Am. Chem. Soc.* **133**, 14510-14513 (2011).
12. Feng X, *et al.* An ambipolar conducting covalent organic framework with self-sorted and periodic electron donor-acceptor ordering. *Adv. Mater.* **24**, 3026-3031 (2012).
13. Calik M, *et al.* Extraction of photogenerated electrons and holes from a covalent organic framework integrated heterojunction. *J. Am. Chem. Soc.* **136**, 17802-17807 (2014).
14. Wan S, Guo J, Kim J, Ihee H, Jiang D. A photoconductive covalent organic framework: Self-condensed arene cubes composed of eclipsed 2D polypyrene sheets for photocurrent generation. *Angew. Chem. Int. Ed.* **48**, 5439-5442 (2009).

15. Wan S, *et al.* Covalent organic frameworks with high charge carrier mobility. *Chem. Mater.* **23**, 4094-4097 (2011).
16. Ding X, *et al.* Synthesis of metallophthalocyanine covalent organic frameworks that exhibit high carrier mobility and photoconductivity. *Angew. Chem. Int. Ed.* **50**, 1289-1293 (2011).
17. Ding H, *et al.* A tetrathiafulvalene-based electroactive covalent organic framework. *Chem. Eur. J.* **20**, 14614-14618 (2014).
18. Chen L, *et al.* Photoelectric covalent organic frameworks: Converting open lattices into ordered donor-acceptor heterojunctions. *J. Am. Chem. Soc.* **136**, 9806-9809 (2014).
19. Feng X, Chen L, Dong Y, Jiang D. Porphyrin-based two-dimensional covalent organic frameworks: Synchronized synthetic control of macroscopic structures and pore parameters. *Chem. Commun.***47**, 1979-1981 (2011).
20. Dogru M, *et al.* A photoconductive thienothiophene-based covalent organic framework showing charge transfer towards included fullerene. *Angew. Chem. Int. Ed.* **52**, 2920-2924 (2013).
21. Guo J, *et al.* Conjugated organic framework with three-dimensionally ordered stable structure and delocalized π clouds. *Nat. Commun.* **4**, 2736 (2013).
22. Colson JW, *et al.* Oriented 2D covalent organic framework thin films on single-layer graphene. *Science* **332**, 228-231 (2011).
23. Medina DD, *et al.* Oriented thin films of a benzodithiophene covalent organic framework. *ACS Nano* **8**, 4042-4052 (2014).
24. Sun B, Li J, Dong WL, Wu ML, Wang D. Selective growth of covalent organic framework ultrathin films on hexagonal boron nitride. *J. Phys. Chem. C* **120**, 14706-14711 (2016).
25. Colson JW, Mann JA, DeBlase CR, Dichtel WR. Patterned growth of oriented 2d covalent organic framework thin films on single-layer graphene. *J. Poly. Sci. A Poly. Chem.* **53**, 378-384 (2015).
26. Spitler EL, *et al.* Lattice expansion of highly oriented 2D phthalocyanine covalent organic framework films. *Angew. Chem. Int. Ed.* **51**, 2623-2627 (2012).
27. DeBlase CR, *et al.* Rapid and efficient redox processes within 2D covalent organic framework thin films. *ACS Nano* **9**, 3178-3183 (2015).
28. Ma L, Yang Y. Unique architecture and concept for high-performance organic transistors. *Appl. Phys. Lett.* **85**, 5084 (2004).
29. Ben-Sasson AJ, Tessler N. Unraveling the physics of vertical organic field effect transistors through nanoscale engineering of a self-assembled transparent electrode. *Nano Lett.* **12**, 4729-4733 (2012).
30. Hlaing H, *et al.* Low-voltage organic electronics based on a gate-tunable injection barrier in vertical graphene-organic semiconductor heterostructures. *Nano Lett.* **15**, 69-74 (2015).
31. Kim K, *et al.* Structural and electrical investigation of C_{60}-graphene vertical heterostructures. *ACS Nano* **9**, 5922-5928 (2015).
32. Liu Y, Zhou HL, Weiss NO, Huang Y, Duan XF. High-performance organic vertical thin film transistor using graphene as a tunable contact. *ACS Nano* **9**, 11102-11108 (2015).
33. Shih C-J, *et al.* Partially-screened field effect and selective carrier injection at organic semiconductor/graphene heterointerface. *Nano Lett.* **15**, 7587-7595 (2015).
34. Lemaitre MG, *et al.* Improved transfer of graphene for gated schottky-junction, vertical,

organic, field-effect transistors. *ACS Nano* **6**, 9095-9102 (2012).
35. Yu Y-J, Zhao Y, Ryu S, Brus LE, Kim KS, Kim P. Tuning the graphene work function by electric field effect. *Nano Lett.* **9**, 3430-3434 (2009).
36. Georgiou T, *et al.* Vertical field-effect transistor based on graphene-WS_2 heterostructures for flexible and transparent electronics. *Nat. Nanotechnol.* **8**, 100-103 (2013).
37. Figueira-Duarte TM, Müllen K. Pyrene-based materials for organic electronics. *Chem. Rev.* **111**, 7260-7314 (2011).
38. Dai W, *et al.* Synthesis of a two-dimensional covalent organic monolayer through dynamic imine chemistry at the air/water interface. *Angew. Chem. Int. Ed.* **55**, 213-217 (2016).
39. Li J, *et al.* Controllable atmospheric pressure growth of mono-layer, bi-layer and tri-layer graphene. *Chem. Commun.* **50**, 11012-11015 (2014).
40. Jiang S, *et al.* Distinguishing adjacent molecules on a surface using plasmon-enhanced raman scattering. *Nat. Nanotechnol.* **10**, 865-869 (2015).
41. Rabbani MG, Sekizkardes AK, Kahveci Z, Reich TE, Ding R, El-Kaderi HM. A 2D mesoporous imine-linked covalent organic framework for high pressure gas storage applications. *Chem. Eur. J.* **19**, 3324-3328 (2013).
42. Lemaitre MG, *et al.* Improved transfer of graphene for gated schottky-junction, vertical, organic, field-effect transistors. *ACS Nano* **6**, 9095-9102 (2012).
43. Britnell L, *et al.* Field-effect tunneling transistor based on vertical graphene heterostructures. *Science* **335**, 947-950 (2012).
44. Das Sarma S, Adam S, Hwang EH, Rossi E. Electronic transport in two-dimensional graphene. *Rev. Modern Phys.* **83**, 407-470 (2011).
45. Sonar P, Singh SP, Li Y, Soh MS, Dodabalapur A. A low-bandgap diketopyrrolopyrrole-benzothiadiazole-based copolymer for high-mobility ambipolar organic thin-film transistors. *Adv. Mater.* **22**, 5409-5413 (2010).
46. Li P, *et al.* D-A1-D-A2 copolymer based on pyridine-capped diketopyrrolopyrrole with fluorinated benzothiadiazole for high-performance ambipolar organic thin-film transistors. *ACS Appl. Mater. Interfaces* **8**, 8620-8626 (2016).
47. Li J, *et al.* Click and patterned functionalization of graphene by diels-alder reaction. *J. Am. Chem. Soc.* **138**, 7448-7451 (2016).
48. Rabbani MG, Sekizkardes AK, El-Kadri OM, Kaafarani BR, El-Kaderi HM. Pyrene-directed growth of nanoporous benzimidazole-linked nanofibers and their application to selective co2 capture and separation. *J. Mater. Chem.* **22**, 25409-25417 (2012).

Acknowledgements

Y.L. and C.Z. acknowledge the support from The Molecular Foundry and Advanced Light Source at

Lawrence Berkeley National Laboratory, respectively, both supported by the Office of Science, Office of Basic Energy Sciences, Scientific User Facilities Division, of the U.S. Department of Energy under Contract No. DE-AC02-05CH11231.

Additional information:

Supplementary Information accompanies this paper at http://www.nature.com/naturecommunications

Competing financial interests: The authors declare no competing financial interests.

Figure Captions

Figure 1 Synthesis of $COF_{TFPy\text{-}PPDA}$ thin film on SLG and the fabrication of VFET device. (a) Schematic diagrams of synthesizing $COF_{TFPy\text{-}PPDA}$ film on SLG transferred onto SiO_2-Si for VFET device fabrication. A sealed tube was charged with a SLG/SiO_2-Si slice as well as the monomers and solvent for COF thin film growth. A COF/SLG-VFET was fabricated based on the SLG-$COF_{TFPy\text{-}PPDA}$-metal stack. (b) Solvothermal reaction for synthesis of $COF_{TFPy\text{-}PPDA}$ in the sealed tube. (c) Side module view of the device geometry of the constructed COF/SLG-VFET device.

Figure 2 Structural characterizations of $COF_{TFPy\text{-}PPDA}$ thin film. (a) Comparison of Fourier transform infrared (FTIR) spectra of $COF_{TFPy\text{-}PPDA}$ film (violet curve), powders (olive curve), TFPy (magenta curve) and PPDA (red curve). (b) Contrastive Raman spectra of $COF_{TFPy\text{-}PPDA}$ film (magenta curve) and powders (blue curve) with the corresponding monomers (TFPy, olive cure and PPDA, red curve) and SLG (black curve).

Figure 3 Crystallinity and orientation $COF_{TFPy\text{-}PPDA}$ thin film on SLG. (a) GIWAXS data of $COF_{TFPy\text{-}PPDA}$ thin film grown on SLG surface. Date scale from 0 to 20000 counts. (b) GIWAXS data obtained at large q_Z showing the projection of $COF_{TFPy\text{-}PPDA}$ (001) peak. (c) Projection of in-plane diffraction pattern from GIWAXS near $q_Z = 0$.

Figure 4 Surface and thickness analysis by using AFM. (a) AFM topography image of $COF_{TFPy\text{-}PPDA}$ film surface. Length scale bar: 2 μm, height scale from -100 to 100 nm. (b) Cross-section analysis of $COF_{TFPy\text{-}PPDA}$ thin film. The monomer concentrations are 5 mM for TFPy and 10 mM for PPDA.

Figure 5 Electrical transport characterization of SLG/COF-VFET. (a) Transfer characteristics of the ambipolar SLG/$COF_{TFPy\text{-}PPDA}$-VFET at V_{DS} values of -0.5, -1.0, and 0.5 V with 50 nm channel

length and 300 nm SiO_2 gate dielectric. (b) Output characteristics of the ambipolar SLG/$COF_{TFPy-PPDA}$-VFET depending on various gate voltages.

Figure 6 Schematic diagram of ambipolar transport behavior. (a) The band diagrams of $COF_{TFPy-PPDA}$ comparing with TFPy. Schematic illustration on (b) the relevant levels of materials in the SLG/COF-VFET and the band diagrams in the case of (c) negative gate voltage and (d) positive gate voltage.

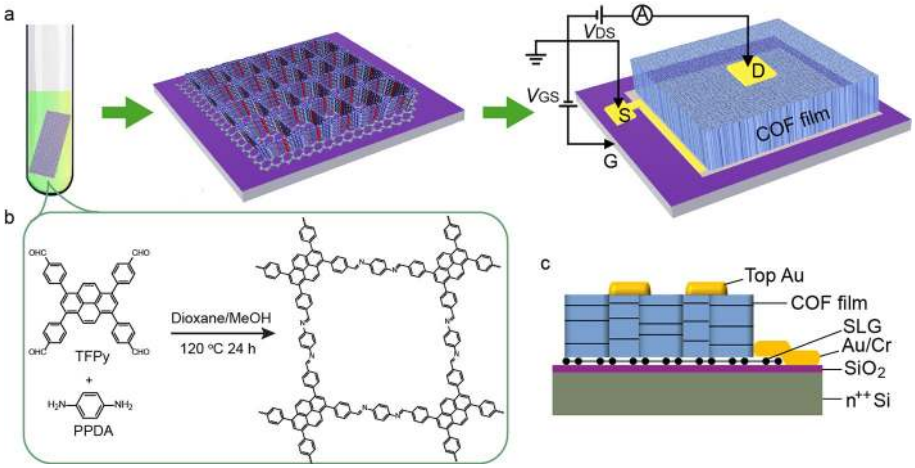

Figure 1

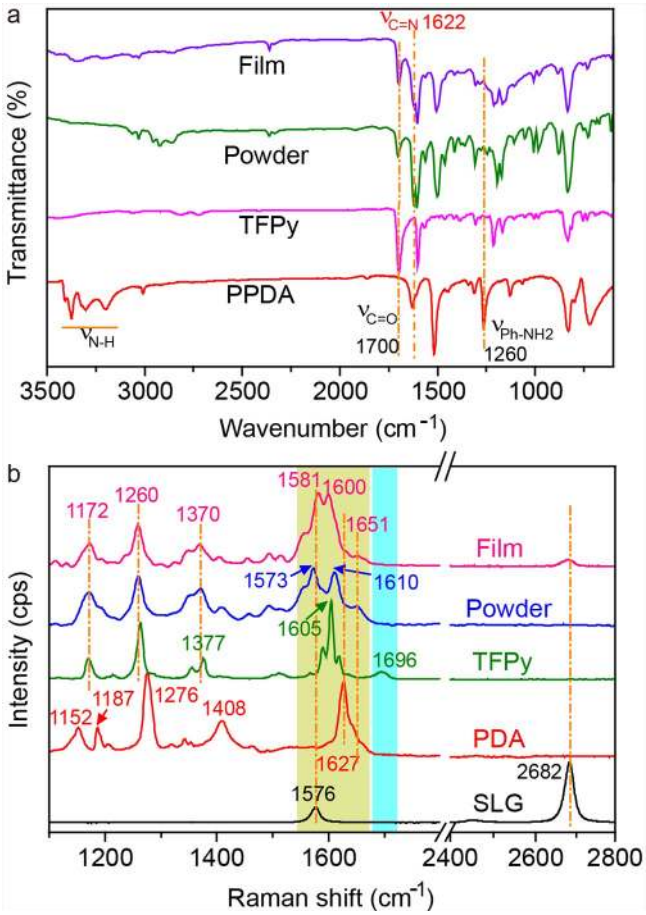
a
Film
Powder
TFPy
PPDA
$\nu_{C=N}$ 1622
$\nu_{C=O}$ 1700
ν_{Ph-NH2} 1260
ν_{N-H}
Transmittance (%)
Wavenumber (cm^{-1})
b
Film
Powder
TFPy
PDA
SLG
Intensity (cps)
Raman shift (cm^{-1})

Figure 2

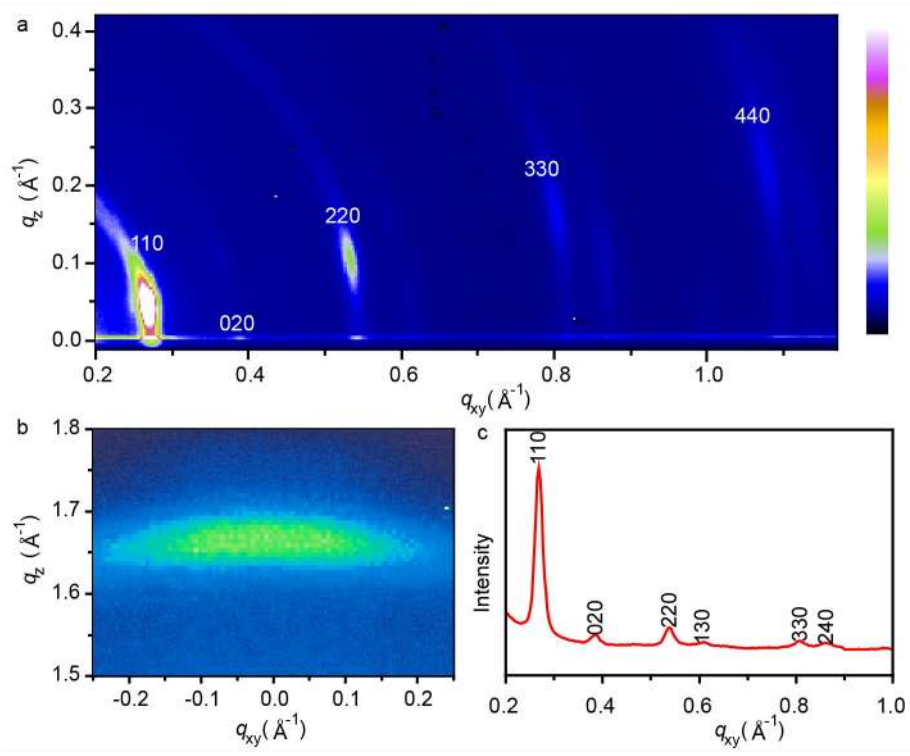
a
110
020
220
330
440
q_z (Å^{-1})
q_{xy}(Å^{-1})
b
q_z (Å^{-1})
q_{xy}(Å^{-1})
c
Intensity
110
020
220
130
330
240
q_{xy}(Å^{-1})

Figure 3

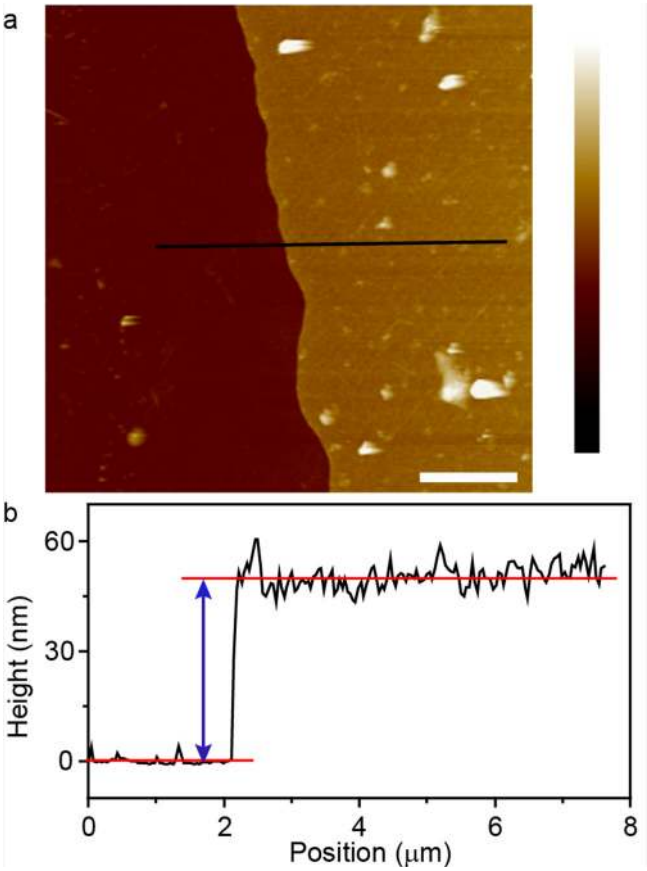

Figure 4

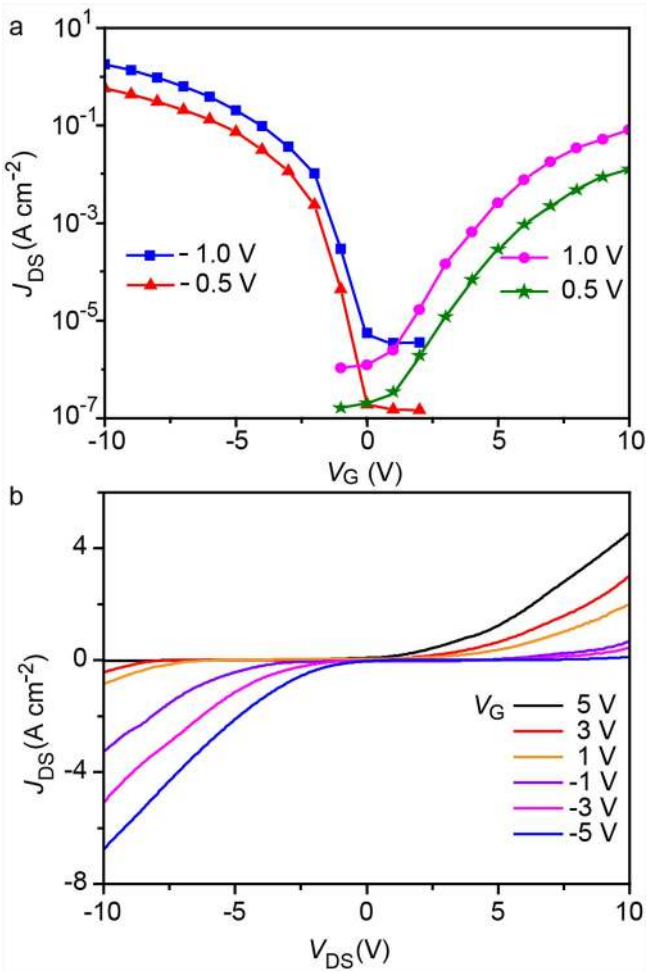

Figure 5

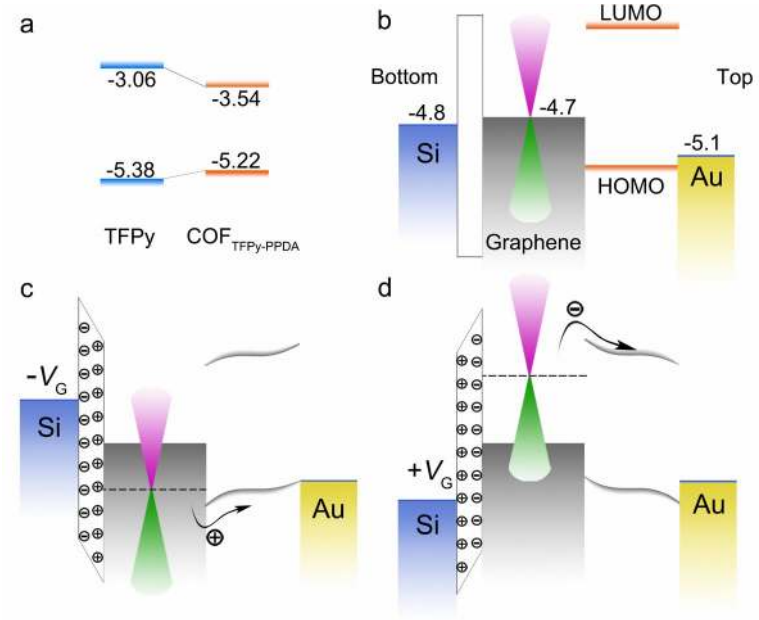

Figure 6